Pergamon

Cement and Concrete Research 32 (2002) 1961–1970

CEMENT AND CONCRETE RESEARCH

The effect of the bond between the matrix and the aggregates on the cracking mechanism and fracture parameters of concrete

G.V. Guinea[a,*], K. El-Sayed[b], C.G. Rocco[c], M. Elices[a], J. Planas[a]

[a]*Departamento de Ciencia de Materiales, Universidad Politécnica de Madrid, E.T.S.I. Caminos, Ciudad Universitaria s/n, Canales y Puertos, 28040 Madrid, Spain*

[b]*Department of Civil Engineering, Benha Higher Institute of Technology, Cairo, Egypt*

[c]*Facultad de Ingeniería, Universidad Nacional de la Plata, La Plata, Argentina*

Received 17 April 2000; accepted 13 June 2002

Abstract

The aggregate–matrix interface plays a leading role in the fracture mechanisms and in the fracture response of concrete. In this work, the influence of the interface on the macroscopic fracture parameters of concrete is investigated. Eleven concrete batches were cast with the same matrix. Different—crushed or rounded—aggregates from the same quarry were used, and several surface treatments were applied to improve or degrade the bond between the matrix and the particles. Fracture tests (three-point bending tests and Brazilian splitting tests) were carried out to determine the fracture energy and other relevant fracture parameters of the concrete batches. The modulus of elasticity and the compressive strength were obtained from uniaxial compression tests. The macroscopic fracture behaviour was modeled by the cohesive crack model with a bilinear softening curve. The results show that concretes with the same matrix and aggregates, and similar behaviour under uniaxial compression, can give very different fracture responses. The work shows how fracture behaviour is governed by the interfacial properties that are also behind the cracking mechanism.

Keywords: Fracture; Aggregate–matrix interface; Concrete

1. Introduction

Plain concrete is a heterogeneous material formed by the combination of hardened cement paste and rocky particles. From a mechanical point of view, plain concrete can be considered as a two-phase material made of a cement-based matrix (mortar) composed of the cement paste and the fine aggregates, and a particulate reinforcement (coarse aggregates). This approach is useful when analyzing the influence of the aggregates on the mechanical performance of concrete, particularly on fracture behaviour, which is known to be affected by the size, shape and grading of the coarser aggregates.

The quality of concrete has been traditionally characterized by the compressive strength, f_c, which has been the key parameter governing the design, manufacture and control of concrete batches. All the major concrete standards [1,2] include empirical formulae to deduce other mechanical properties from f_c, such as the modulus of elasticity or the tensile strength. Nevertheless, an increasing amount of experimental evidence, particularly during the last decade, has shown that such empirical approximations are applicable only within a narrow range of compositions. This is especially significant when fracture properties such as the tensile strength or the fracture energy are considered [3].

Many experimental studies have examined the influence of aggregates on the fracture parameters of concrete, mainly concentrating on the effects of the maximum aggregate size and on the quality of the aggregate [3–7].

The dependence of fracture behaviour on the maximum aggregate size, d_{max}, has been observed by many authors, although the large scatter usually present in the results makes it difficult to arrive at definite conclusions. Based on the results of a comparative study organized by RILEM-TC50, Hillerborg [7] concluded that the fracture energy tends to increase as the maximum aggregate size becomes larger. The

* Corresponding author. Tel.: +34-91-336-66-79; fax: +34-91-336-66-80.

E-mail address: gguinea@mater.upm.es (G.V. Guinea).

0008-8846/02/$ – see front matter © 2002 Elsevier Science Ltd. All rights reserved.
PII: S0008-8846(02)00902-X

Table 1
Composition of the concrete batches

Batch	Aggregate coating	Matrix	Aggregate shape
N	–	Normal	–
H	–	Modified	–
NEC	Bitumen emulsion	Normal	Crushed
NPC	Paraffin	Normal	Crushed
N0C	None	Normal	Crushed
NXC	Epoxy resin	Normal	Crushed
NER	Bitumen emulsion	Normal	Rounded
NPR	Paraffin	Normal	Rounded
N0R	None	Normal	Rounded
H0C	None	Modified	Crushed
H0R	None	Modified	Rounded

same trend was reported by Mihashi et al. [3,8] who also analyzed the effect of d_{max} on the softening curve.

Despite the fact that the interface between aggregate and mortar is known to have a remarkable effect on the tensile properties of concrete [9], few experimental analyses have been carried out to clarify its influence. Depending on the strength of the interface relative to the aggregate and to the matrix, a crack will propagate either through the particles or around them, producing a different crack roughness. The type of propagation influences the energy consumption and the interlock effects, and has a direct effect on concrete toughness.

In this paper, experimental results are presented to show the influence of the aggregate–matrix interface on the fracture parameters of concrete. The influence of the shape of the aggregates—usually affecting the interfacial strength—is also investigated. The macroscopic fracture behaviour of concrete is characterized by means of the cohesive crack model [10], which has shown its utility in modeling the fracture process in concrete and concrete-like materials when the failure mode is governed by a single macrocrack [11,12]. Using the cohesive crack model as a framework, the effect of the interface on the tensile strength, f_t, on the fracture energy, G_F, and on the complete softening curve is given.

The materials and specimens used in this work, and the tests performed, are presented in the following section. Eleven concrete batches were cast with the same matrix and type of aggregate, but with varying quality of the interface, and three-point bending fracture tests and Brazilian splitting tests were carried out to determine the fracture energy and other relevant parameters. Section 3 shows the fracture characterization of the batches, their properties and the shape of the softening curve—based on the application of the cohesive crack model, and a topographical analysis of the cracked surfaces. On the basis of these results, the influence of the interface and of the shape of the aggregates is highlighted in Section 4, which draws the main conclusions and closes the paper.

2. Materials and tests

2.1. Materials and specimens

Concrete specimens were made with ordinary Portland cement (ASTM Type I) and siliceous aggregates. Silica sand with a grading within ASTM C33 standard limits and a maximum size of 2 mm was used as fine aggregate for the matrix. The coarse aggregate was formed of rounded or crushed granite particles from a single size fraction of 5–7 mm. To preserve the properties of the parent rock, crushed particles were obtained by grinding oversized fractions of rounded aggregates.

Eleven batches were cast, as summarized in Table 1. The volume fraction of the coarse aggregate was kept constant in all the batches at 40%. Two different matrixes, normal (N) and modified (H), were used to promote or inhibit the debonding of the aggregates. The cement, sand and water content of the two matrixes are given in Table 2, which also shows the use of a superplasticizer (Sikament 300) to improve the workability. Silica fume was added to matrix (H) to enhance the bond between the matrix and the aggregates.

Three surface treatments were used to improve/weaken the interface between the coarse aggregates and the matrix. Bitumen and paraffin coatings were applied to weaken the bond, and an epoxy resin to increase it. All the coatings were dosed by weight, equal to 5% of the coarse aggregate.

In addition, two shapes for the coarse aggregate—rounded and crushed—were considered.

Four prismatic specimens of $40 \times 40 \times 180$ mm^3 were cast from each concrete batch. After demoulding, samples were stored under lime-saturated water at 20 ± 3 °C to prevent microcracking until the time of the test. Before testing, a central notch, 2 mm wide, was sawn up to 25% of the specimen depth (10 mm).

2.2. Mechanical characterization

Three sets of experiments were carried out to characterize the mechanical behaviour for each concrete batch: stable

Table 2
Mix proportions

Matrix	Cement (kg/m^3)	Sand (kg/m^3)	Water (kg/m^3)	Superplasticizer (kg/m^3)	Silica fume (kg/m^3)	$\frac{\text{Water}}{\text{Cement+Silica fume}}$
Normal (N)	832	1121	274	25	–	0.33
Modified (H)	750	1121	274	23	83	0.33

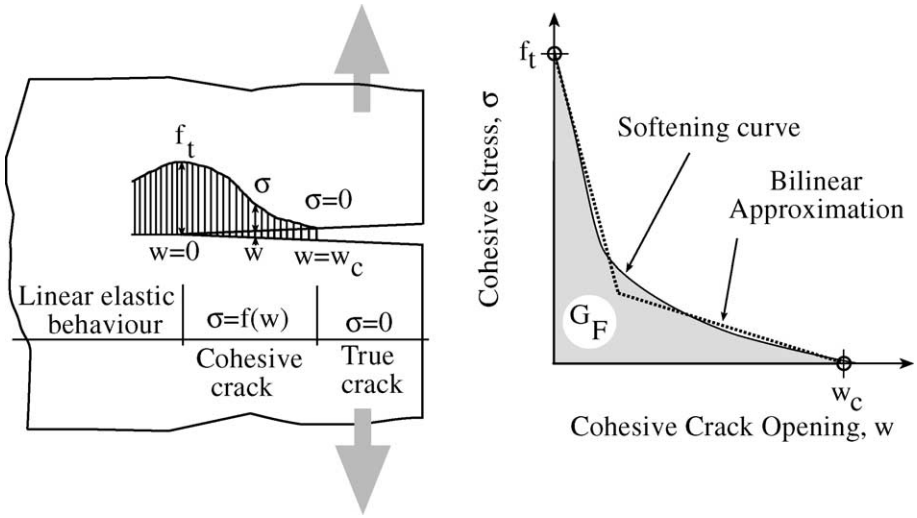

Fig. 1. Cohesive crack and softening function.

three-point bend fracture tests, standard compression tests and Brazilian splitting tests.

Three-point bend tests on quarter-notched beams were performed following the RILEM method [13], enhanced with some additional suggestions by the authors [14–16]. Beams of 40 mm depth were tested in bending, with a span-to-depth ratio of 4. During the test, load-point displacement and crack mouth opening displacement (CMOD) were continuously recorded. The fracture energy, G_F, the critical crack opening, w_c, and the shape of the bilinear softening curve were determined by the method proposed by the authors [17], and are shown in the next section.

Compression tests were performed according to ASTM C39 and ASTM C469 standards to measure the compressive strength, f_c, and the modulus of elasticity in compression, E_c. The test specimens were prisms $40 \times 40 \times 80$ mm^3 cut from the broken halves of the bending tests.

Brazilian splitting tests to measure the tensile strength, f_t, were conducted on $40 \times 40 \times 40$ mm^3 cubes also cut from the specimens tested in bending. The splitting tests followed the guidelines prescribed in the ASTM C496 standard except for the size of the specimen and the width of the load-bearing strips, which was equal to 3 mm—7.5% of the specimen depth. Previous work by the authors has shown that the standardized width of 16% of the specimen depth is usually overdimensioned, and can lead to an erroneous estimation of f_t [18,19].

3. Fracture characterization

3.1. Macroscopic behaviour: the cohesive crack model

Several linear and nonlinear fracture theories have been proposed to model the fracture behaviour of plain concrete when the failure is governed by the development of a single macrocrack. The cohesive—or fictitious—crack is one of the models which best describes the nonlinear fracture

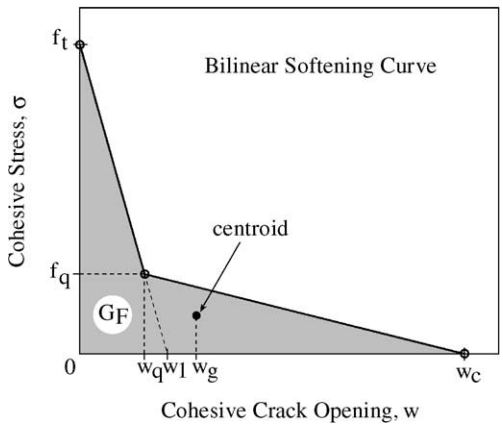

Fig. 2. Bilinear softening function and characteristic parameters.

Table 3
Mechanical properties of the concretes investigated. Mean values and 68% confidence interval

Batch	f_c (MPa)	E_c (GPa)	f_t (MPa)	G_F (J/m^2)
N	71.1 ± 0.2	34.3 ± 0.1	4.00 ± 0.10	67.2 ± 2.0
H	67.6 ± 0.6	31.4 ± 0.3	4.04 ± 0.09	69.5 ± 1.2
NEC	21.0 ± 0.3	19.7 ± 0.7	2.19 ± 0.03	125.8 ± 6.3
NPC	36.1 ± 1.3	25.6 ± 0.6	2.99 ± 0.10	141.1 ± 9.0
N0C	73.2 ± 2.0	33.1 ± 0.8	4.15 ± 0.05	136.0 ± 4.8
NXC	67.0 ± 0.9	34.3 ± 0.3	4.16 ± 0.08	134.3 ± 6.3
NER	21.9 ± 0.5	22.5 ± 0.5	2.46 ± 0.07	67.8 ± 2.5
NPR	41.5 ± 0.8	33.7 ± 0.6	3.11 ± 0.04	77.0 ± 6.7
N0R	63.8 ± 2.6	39.8 ± 1.0	3.93 ± 0.05	94.7 ± 5.7
H0C	87.5 ± 0.3	34.7 ± 0.5	4.89 ± 0.12	127.5 ± 6.6
H0R	67.6 ± 3.5	40.0 ± 0.4	4.93 ± 0.10	87.1 ± 3.8

Table 4
Characterization of the cracked surfaces: % area of broken and debonded particles (coarse aggregate only) and roughness parameters. Mean values and 68% confidence interval

Batch	% Broken	% Debonded	R_a (mm)	R_q (mm)
N	–	–	0.306 ± 0.001	0.388 ± 0.007
H	–	–	0.495 ± 0.024	0.595 ± 0.029
NEC	3.4 ± 0.5	46.6 ± 0.9	Not measured	Not measured
NPC	6.2 ± 1.0	38.6 ± 2.1	0.901 ± 0.080	1.097 ± 0.070
N0C	17.3 ± 1.2	18.1 ± 1.6	1.146 ± 0.169	1.338 ± 0.183
NXC	12.0 ± 1.4	27.2 ± 1.5	Not measured	Not measured
NER	3.7 ± 0.6	48.6 ± 0.1	Not measured	Not measured
NPR	4.8 ± 1.0	38.3 ± 1.9	1.075 ± 0.218	1.278 ± 0.241
N0R	12.0 ± 0.4	27.4 ± 1.7	0.972 ± 0.013	1.177 ± 0.007
H0C	22.2 ± 1.2	9.5 ± 0.9	0.577 ± 0.081	0.708 ± 0.100
H0R	12.0 ± 1.5	25.0 ± 0.7	0.972 ± 0.013	1.177 ± 0.007

processes. The first applications of this model to concrete were those by Hillerborg et al. [10], and since then it has been used successfully to explain many experimental results in concrete, ceramics and rocks. The basic properties of a cohesive crack are reviewed in Refs. [11,12].

The cohesive crack model introduces the softening function to simulate the microcracking and deterioration of the material in the fracture process zone, which is modeled by means of a cohesive crack, which can transfer stress—the cohesive stress—from one face to the other. For a crack monotonically loaded in Mode I—the most common testing situation—the cohesive stress at a given point σ is normal to the crack faces and is uniquely given by the softening curve as a function of the crack opening at this point w, $\sigma = (w)$, as shown in Fig. 1. The softening function relates the stress transferred between the crack faces to the crack opening at this point, and is considered *by hypothesis* to be a material property, independent of geometry and size.

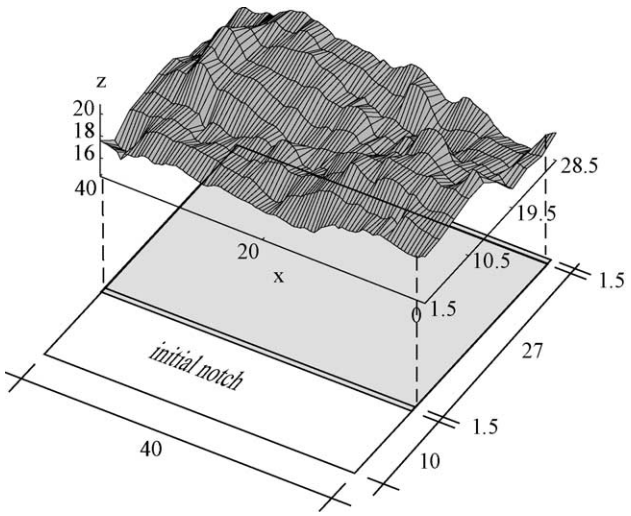

Fig. 3. Topographical view of one of the cracked faces of NPR-3 bending specimen. For clarity, only points with $\Delta x = 0.4$ mm are plotted. Values are in millimeters.

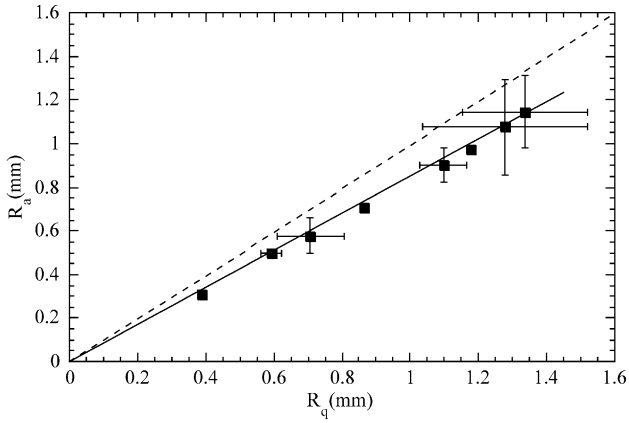

Fig. 4. Correspondence between the average roughness (R_a) and the RMS roughness (R_q).

The stress at the tip of the cohesive crack is equal to the tensile strength of the material, f_t, and decreases progressively as the crack opening increases. When the crack opening reaches the critical crack opening w_c, the cohesive stress drops to zero and a *true*—stress free—crack propagates. The work done to produce a unit area of true crack is the specific fracture energy—or simply fracture energy—G_F, and coincides with the area under the softening curve.

To simplify the computations, the bulk behaviour is assumed to be linear-elastic, although this approximation can be relaxed if necessary.

The fracture energy, G_F, the tensile strength, f_t, the critical crack opening, w_c, and the softening function itself, are all macroscopic material properties, and thus are dependent on the internal structure of the concrete. It is usually assumed that the size of the coarse aggregate and the crack roughness are responsible for the transfer of cohesive stresses at large crack openings at the tail of the softening curve. Also, it is assumed that the initial steeper portion of the softening curve is controlled by the cracking in the matrix. Nevertheless, no direct and quantitative evidence has been given to support these statements.

In this work, the softening function is approximated by a bilinear function (Fig. 2). This simple diagram suffices to describe the prepeak as well as the postpeak behaviour of the material, as many authors have pointed out [1,4]. The four parameters needed for the bilinear approximation can be easily determined following the fitting procedure by the authors [17], which makes use of the results of stable three-point bending tests on notched beams and of the Brazilian splitting test. The primary output of the fitting procedure gives the tensile strength, f_t—from the splitting tests—the horizontal intercept of the initial tangent, w_1, the area under the softening curve, G_F, and the position of the centroid of the softening curve, w_g, these last three obtained from the stable bending test as explained in Ref. [17]. From f_t, w_1, G_F and w_g the critical crack opening w_c and the position of the kink point (w_q, f_q) (Fig. 2) can be readily obtained.

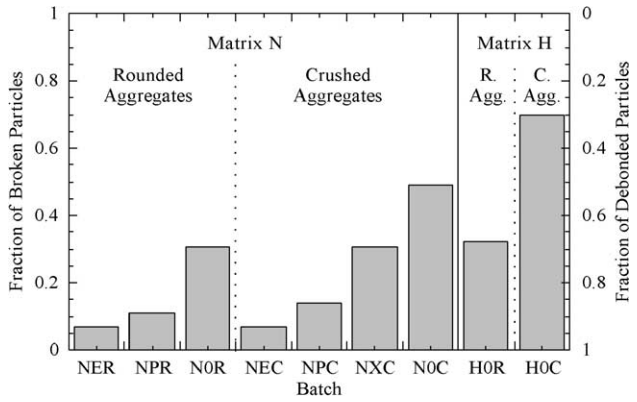

Fig. 5. Fraction of broken/debonded particles for the concretes investigated. The identification of the batches is given in Table 1.

The basic mechanical properties of the 11 batches investigated are given in Table 3. In Section 4, the fracture properties are analyzed in relation to the quality of the interface between the matrix and the aggregates.

3.2. Crack surface characterization

The cracked surfaces of the specimens tested under three-point bending were analyzed to obtain their composition and topography. The projected area of broken and debonded particles was optically measured on all the specimens tested and the results are given in Table 4. The specific area taken by the coarse aggregate—broken and debonded particles—was very similar in all the batches, roughly 45% of the ligament, as deduced from Table 4.

The topographic analysis of the crack surfaces produced by the three-point bend tests was performed by means of a laser profilemeter. Ten profiles, 3 mm spaced and parallel to the crack front, were measured on one of the cracked halves of the specimens. The profile points were recorded every 20 μm along the path, with a resolution of 3 μm in height. Fig. 3 shows one of the surfaces measured.

The average roughness, R_a, and the RMS roughness, R_q, were calculated for every concrete batch. These standard amplitude parameters are conventionally defined as [20] (Eqs. (1) and (2)):

$$R_a = \frac{1}{L}\int_0^L |z(x)|\mathrm{d}x \tag{1}$$

$$R_q = \sqrt{\frac{1}{L}\int_0^L z^2(x)\mathrm{d}x} \tag{2}$$

where L is length of the projected profile, and $z(x)$ is the centre-line profile, which satisfies (Eq. (3)):

$$0 = \int_0^L z(x)\mathrm{d}x \tag{3}$$

The mean roughness of each specimen was computed by averaging the 10 values—one for every profile—of R_a and R_q measured on the specimen. The roughness of each concrete batch was obtained as the average of the four specimens tested per batch. Due to the large amount of data involved—close to 20.000 points per specimen analyzed—only the two matrixes, N and H, the H0C and H0R concretes, and the batches NP* and N0* were considered. The reason for selecting these batches was to analyze concretes exhibiting extreme behaviour, with most of their particles broken or debonded, as shown in Table 4 which gives the results.

The roughness parameters, R_a and R_q show good correspondence for the groups analyzed, as displayed in Fig. 4. The RMS roughness, R_q, gave systematically higher values than R_a.

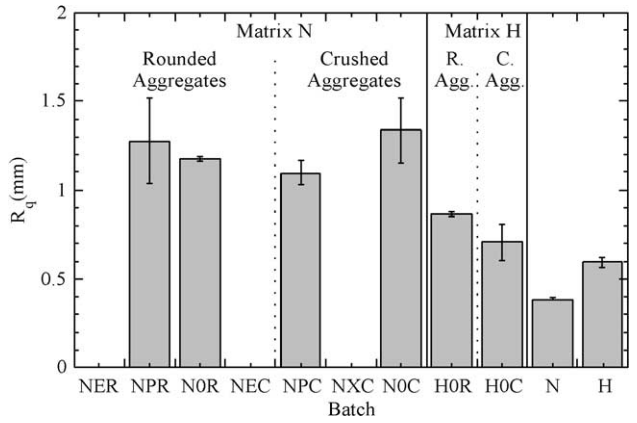

Fig. 6. RMS roughness, R_q, for the concretes investigated. The identification of the batches is given in Table 1.

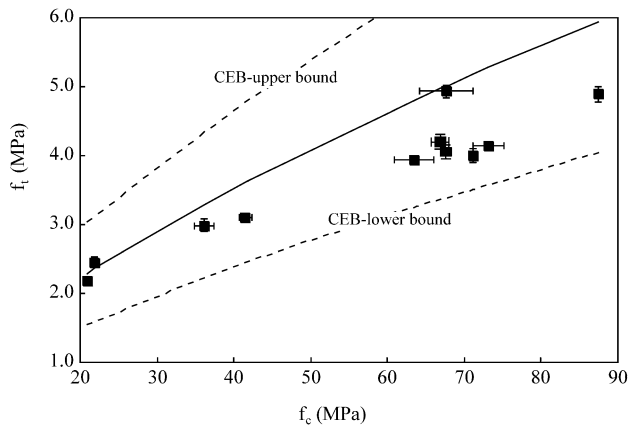

Fig. 7. Relation between tensile and compressive strength.

4. Results and discussion

4.1. Cracking mechanism

Fig. 5 shows the fraction of broken particles of coarse aggregate in the 11 concretes fabricated. The area of broken particles increases as the interface becomes stronger. The minimum area of broken particles—the maximum debonded area—is obtained in concretes with a weak interface produced by coating with bitumen or paraffin. In these concretes, most of the aggregates—up to 93%—debond during the fracture process, irrespective of whether they are rounded or crushed.

The natural interface between the siliceous aggregate and the mortar was found to be a strong joint, even more than when the aggregate is coated with epoxy resin. With this kind of interface, crushed aggregates perform better, and the debonded fraction is reduced by up to 50%.

The partial replacement of cement by silica fume in matrix H improves the bond between the matrix and the aggregates, and produces the highest fractions of broken areas for both crushed and rounded particles. The extreme situation is reached by H0C concrete, with crushed aggregates, in which the debonded area is reduced by up to 30% of the total area of particles present in the crack surface.

The roughness of the cracked surfaces is not well correlated with the main cracking mechanism—breaking or debonding of the aggregates—as is shown in Fig. 6. Concretes with the same matrix N and rounded or crushed aggregates behave in opposite ways: in batches with rounded particles, R_q remains constant or diminishes slightly as the interface becomes stronger and the broken fraction of particles increases, whereas the opposite trend is observed in concretes with crushed aggregates. The influence of rounded or crushed aggregates also gives dissimilar trends in the case of concretes with matrix N or H, and the larger roughness of matrix H itself as compared with matrix N does not correlate well with the measures in concrete batches, those with matrix N giving the higher values.

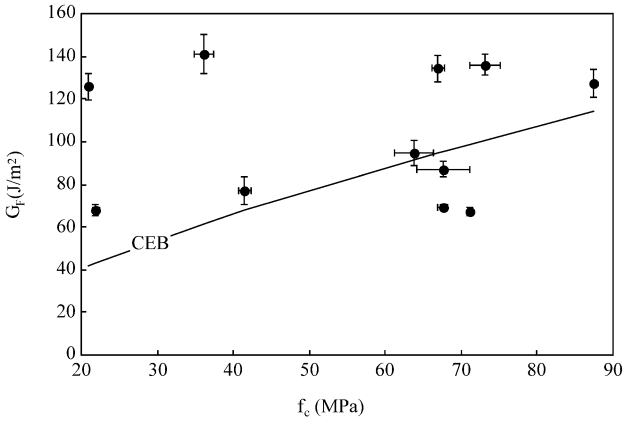

Fig. 9. Relation between fracture energy and compressive strength.

4.2. Compressive strength and modulus of elasticity in compression

The classical properties f_c, and E_c are clearly affected by the quality of the interface, as demonstrated by the values in Table 3. A weak interface results in a sensible reduction in f_c, which can go well below 30% of the strength of a good bond. Conversely, the improvement of the interface can increase f_c over the matrix strength if the aggregate is strong enough. This situation is illustrated in Table 3 with H0C concrete, where the strength of the matrix is increased by 30% with the inclusion of crushed aggregates.

This behaviour is associated with the inclusion of weak points in the matrix—the interfaces between mortar and aggregates—where the cracks can initiate. The strength of the interface between the aggregates and the matrix promotes or restrains the nucleation and propagation of these cracks, and influences the structural strength. The use of

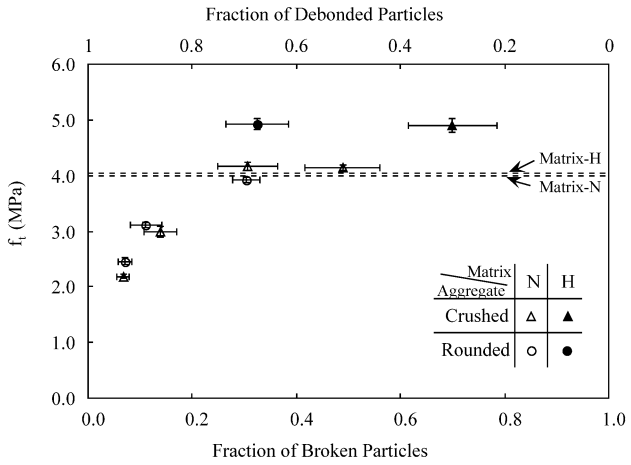

Fig. 8. Variation of the tensile strength with the fraction of broken particles.

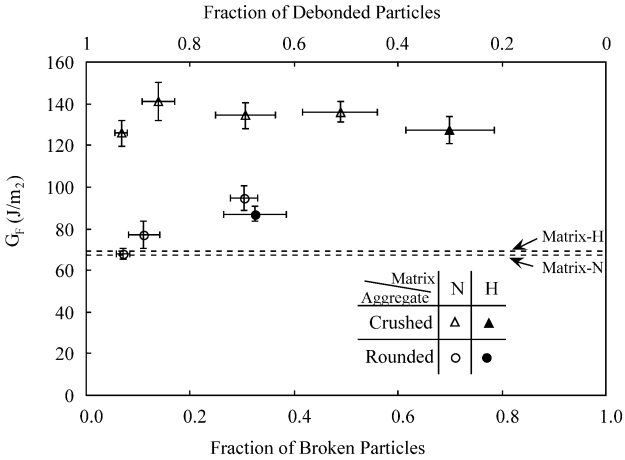

Fig. 10. Variation of the fracture energy with the fraction of broken particles.

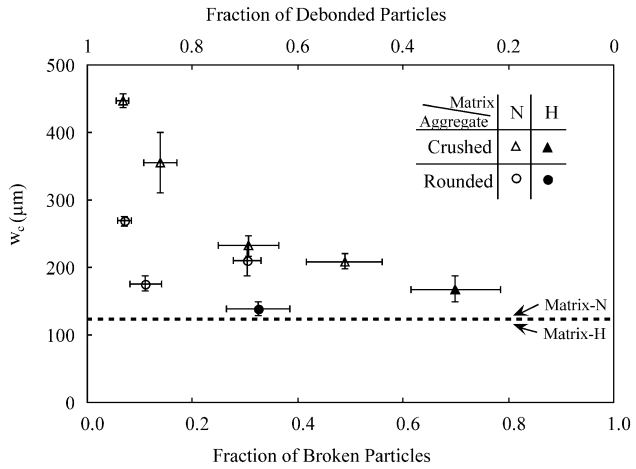

Fig. 11. Variation of the critical crack opening with the fraction of broken particles.

crushed aggregates produces stronger interfaces, and concretes with this kind of aggregate are those with the highest values of f_c in Table 3.

The modulus of elasticity is also affected to a large extent by the quality of the interface, and Table 3 shows that E_c can vary by up to 50%. The effect of the aggregate in this case is of second order, and differences between batches with crushed and batches with rounded aggregates are within a 10% variation.

4.3. Tensile strength

The relationship between the tensile and the compressive strengths obtained in the experiments are in accordance with the trends suggested by the CEB Model Code [1] (shown in Fig. 7). The values for concretes with very different rupture mechanisms—breaking or debonding of the aggregates—fall between the upper and the lower limits recommended in the standard. Nevertheless, the mean value for f_t recommended in the CEB Model Code (Eq. (4)):

$$f_t = 1.40\left(\frac{f_c}{10\ \text{MPa}}\right)^{2/3} \quad \text{MPa} \tag{4}$$

with f_c in (MPa), overestimates the tensile strength, in particular, when the bond between the matrix and the aggregate is good.

Fig. 8 shows the influence of the interface on the tensile strength. For the ordinary matrix (N), the modification of the bond between the particles and the matrix makes f_t vary by a factor close to 2, and the matrix strength seems to be the upper limit, as reported in other published works [9]. Results in Fig. 8 suggest that the effect of the interface is appreciable only when the fraction of broken particles is under 20%, otherwise f_t is practically unaffected. No significant differences come up between the use of crushed and the use of rounded aggregates.

A remarkable fact from Fig. 8, not usually reflected in the literature, is that the use of an adherent matrix (H) can improve f_t to well over the matrix strength.

4.4. Fracture energy

Fig. 9 shows the fracture energy, G_F, in terms of the compressive strength. From this figure, it is concluded that G_F is not directly correlated with f_c, according to earlier results published by Mihashi [3]. Our results clearly show that all the estimation formulae for G_F based on a definite correlation with f_c are inapplicable. Among them, the CEB formula, which is also plotted in Fig. 9, and that for concretes with maximum aggregate size of 8 mm, is given by (Eq. (5)):

$$G_F = 25\left(\frac{f_c}{10\ \text{MPa}}\right)^{0.7} \quad \text{J/m}^2 \tag{5}$$

with f_c in MPa. This formula does not take into account the different energy consumption produced by the cracking mechanism when the crack front breaks or debonds the aggregates, and is a lower bound for most concretes.

The strength of the interface affects the fracture energy in different ways depending on the shape of the particles. This is shown in Fig. 10 where concretes with crushed aggregates have a higher G_F, as was shown by the authors in a previous work [21]. For this kind of concrete, the interface has no influence on the fracture energy, possibly due to fact that the decrease in energy consumption by the interfaces is offset by the interlock mechanisms at the end of the softening curve (revealed by a larger critical crack opening, w_c, as commented later in Section 4.5).

A less efficient interlock mechanism for the concretes with rounded particles—which have shown lower values of w_c—will result in a reduction of G_F when the fraction of debonded aggregates increases, as is shown in Fig. 10.

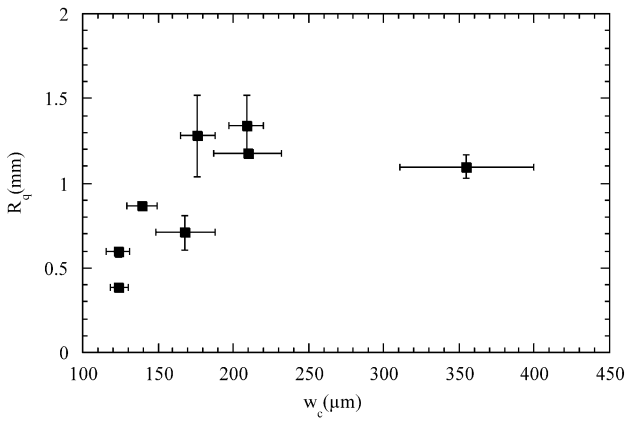

Fig. 12. Relation between the RMS roughness and the critical crack opening.

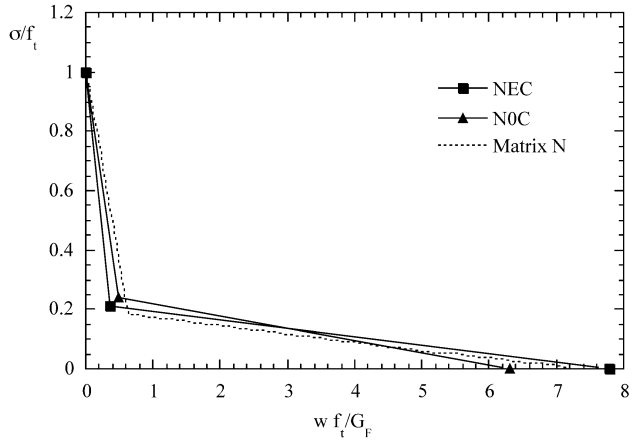

Fig. 13. Influence of the interface of crushed aggregates on the softening curve.

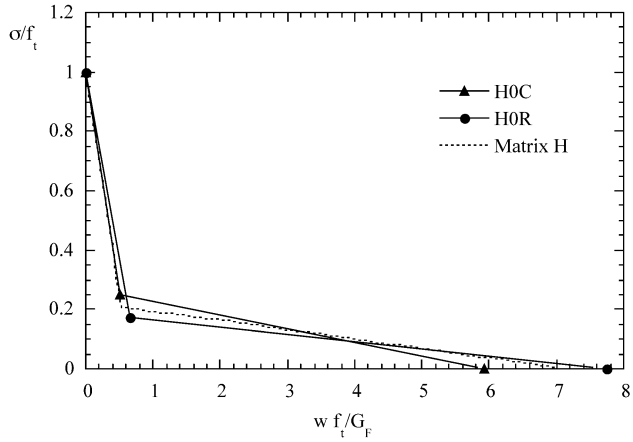

Fig. 14. Influence of the shape of aggregates on the softening curve.

In all the batches, the addition of strong particles to the matrix improved the fracture energy, and this effect was particularly important in concretes with crushed aggregates, where G_F was double that of the matrix.

4.5. Critical crack opening

The critical crack opening, w_c, is the value at which the transferred stress between the cohesive crack faces drops to zero (see Fig. 1). This parameter accounts for all the stress-transferring mechanisms present in concrete, such as aggregate interlocking or crack overlapping [4,10].

The dependence of w_c on the matrix–aggregate interface is shown in Fig. 11. With both crushed and rounded aggregates, w_c decreases as the fraction of broken particles increases, approaching the value corresponding to the matrix, which appears to be the lower bound. This behaviour is congruent with an increment of the interlock mechanism produced by the debonding of aggregates. Concretes with debonded crushed aggregates, where the interlock is extreme, show the highest values of w_c, up to 3.5 times greater than that of the matrix. These values are probably responsible for the constancy of G_F with respect to the fraction of broken/debonded particles shown in Fig. 10. The active interlock mechanism neutralizes the reduction in fracture energy due to a weaker interface.

The critical crack opening, w_c, seems to be correlated with R_q, the RMS roughness, in spite of the large scatter present, as shown in Fig. 12. Only the results for NPC concrete give an abnormally low value for R_q, the general trend being an increase of w_c with the crack roughness.

4.6. Softening curve

The nondimensional softening curves are used to compare systematically the different batches. In these representations, the cohesive stress is referenced to the tensile strength, f_t, and the crack opening is divided by G_F/f_t, the characteristic crack opening. The area under the nondimensional curve—the nondimensional fracture energy—is equal to unity.

Fig. 13 plots the nondimensional softening function for the two concretes with crushed aggregates which have shown extreme behaviour (see Fig. 5): the NEC concrete batch, with most of the particles debonded (93%), and the N0C batch where a large number of the aggregates were broken (49%). Fig. 13 also shows the softening curve corresponding to the common matrix N. The initial part of the softening is very similar in the two concretes and in the mortar matrix. The differences emerge at the tail of the softening curve where the concrete with the weaker interface displays a larger critical crack opening.

The influence of the shape of the aggregate is shown in Fig. 14, where H0C and H0R concretes are compared. When the aggregate is crushed, the softening function displays a shorter tail—in nondimensional terms—while keeping nearly the same initial descending part. This result is congruent with that of Fig. 13 because H0R concrete manifested a weaker interface than H0C (see Fig. 5). As

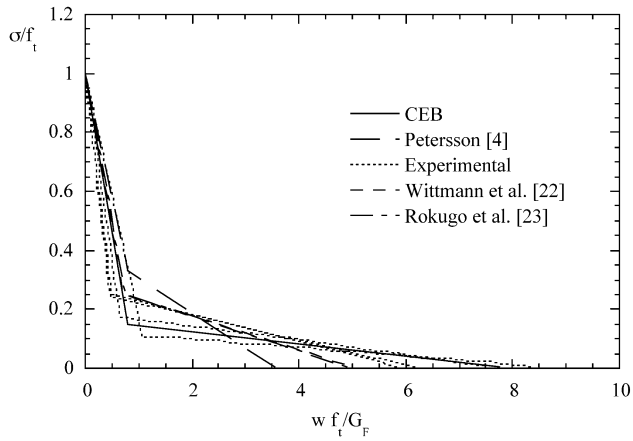

Fig. 15. Comparison between softening curves [22,23].

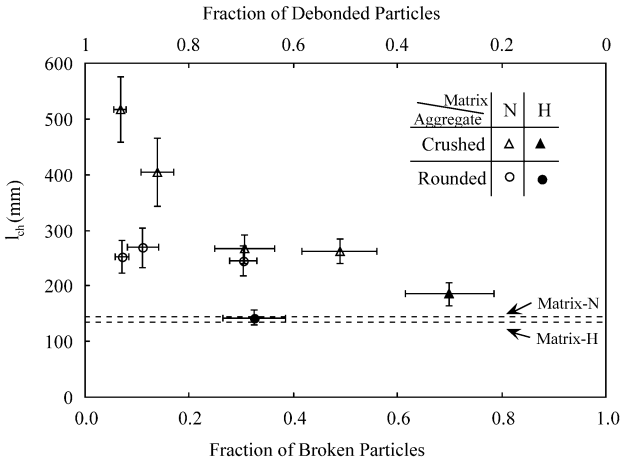

Fig. 16. Variation of the characteristic length with the fraction of broken particles.

in Fig. 13, the matrix behaviour was in between the other two curves.

Results in Figs. 13 and 14 suggest that the initial part of the softening curve is basically controlled by the matrix, and that the interface becomes relevant at the tail of the softening function where a weak interface produces higher values of the dimensionless critical crack opening, $w_c f_t/G_F$.

The experimental curves are compared in Fig. 15 with other curves proposed in the literature. The CEB proposal for a maximum aggregate size of 8 mm—applicable to the concretes analyzed—gives a good representation of the mean fracture behaviour. Petersson's bilinear curve correctly models the initial part but shows a too short tail, as pointed out by the authors [12]. The same comment is applicable to the other proposals.

4.7. Characteristic length

The characteristic length was first defined by Hillerborg et al. [10] as (Eq. (6)):

$$l_{ch} = \frac{EG_F}{f_t^2} \tag{6}$$

where E is the modulus of elasticity, f_t is the tensile strength and G_F is the fracture energy. This parameter is directly related to the cohesive zone extension during the fracture process, and is commonly used to characterize the brittleness of concrete [12]. The smaller the l_{ch} value, the more brittle the material.

As Fig. 16 shows, l_{ch} decreases when the interface becomes stronger and the fraction of broken particles increases. This effect is marked in concretes with crushed aggregates while batches with rounded particles show no significant variation as the interface is modified. In general terms, the effect of the aggregates is favourable, improving the toughness of the matrix.

5. Conclusions

A large experimental work shows the influence of the interface between matrix and aggregates in the fracture properties of concrete. The conclusions to be drawn from this study can be summarized as follows:

- The compressive strength and the modulus of elasticity are strongly affected by the quality of the interface, resulting in a sensible reduction (up to 70% for f_c, and 50% for E_c) when the bond is poor.
- The same trend applies to the tensile strength, f_t, which can vary by a factor close to 2. It appears that the influence of a weak interface is only noticeable when the broken particles are below a certain value, typically 20%. The use of an adherent matrix can improve f_t well over the matrix strength.
- The strength of the interface affects the fracture energy in different ways depending on the shape of the particles. Concretes with crushed aggregates show a higher value of G_F, and the interface has no noticeable effect, possibly due to a more pronounced interlock at the end of the softening curve which compensates the loss of energy consumption in weak interfaces. This effect is not observed in concretes with rounded particles, which display a reduction of G_F when the fraction of debonded aggregates increases.
- The critical crack opening decreases when the interface is strong, approaching the value corresponding to the matrix, and it increases when the crack is rough.
- The initial part of the nondimensional softening curve seems to be controlled by the matrix. The interface between matrix and aggregates influences the tail of the softening, producing higher values of the dimensionless critical crack opening, $w_c f_t/G_F$ when the bond is weak. The experimental curves obtained in this work compare well with other model curves proposed in the literature, the CEB giving the closest fit.
- The material toughness—in terms of l_{ch}, the characteristic length—decreases when the interface becomes stronger, this effect being more marked in concretes with crushed aggregates.

Acknowledgements

The authors gratefully acknowledge support for this research provided by the Spanish Comisión Interministerial de Ciencia y Tecnología (CICYT), under grants MAT 2000-1355 y and MAT 2001-3863-C3-1.

References

[1] CEB-FIP Model Code 1990-Final Draft, Comite Euro-International du Beton, Bulletin d'Information 203, 1991.
[2] ACI-318R, ACI Manual of Concrete Practice, American Concrete Institute, Farmington Hills, MI (USA), 1993.
[3] H. Mihashi, Material structure and tension softening properties of

concrete, in: Z.P. Bazant (Ed.), Fracture Mechanics of Concrete Structures, Elsevier, Colorado, USA, 1992, pp. 239–250.
[4] P.E. Petersson, Crack growth and development of fracture process zone in plain concrete and similar materials, Report TVBM-1006, Division of Building Materials, Lund Institute of Technology, Lund, Sweden, 1981.
[5] H.A.W. Cornelissen, D.A. Hordijk, H.W. Reinhardt, Experiments and theory for the application of fracture mechanics to normal and lightweight concrete, in: F.H. Wittmann (Ed.), Fracture Toughness and Fracture Energy of Concrete, Elsevier, Amsterdam, 1986, pp. 565–575.
[6] M. Elices, G.V. Guinea, J. Planas, Choosing the right concrete for piles: An application in concrete fracture mechanics, in: Z.P. Bazant (Ed.), Fracture Mechanics of Concrete Structure, Elsevier, Colorado, USA, 1992, pp. 782–787.
[7] A. Hillerborg, Results of three comparative test series for determining the fracture energy GF of concrete, Mater. Struct. 18 (1985) 407–413.
[8] H. Mihashi, K. Kirikoshi, N. Nomura, K. Otsuka, Y. Kaneko, Microcracking behaviour and softening properties of concrete, in: H. Mihashi, K. Rokugo (Eds.), Fracture Mechanics of Concrete Structures, Aedificatio Publishers, Freiburg, Germany, 1998, pp. 181–192.
[9] A.M. Neville, Properties of Concrete, Pitman, London, 1981.
[10] A. Hillerborg, M. Modéer, P.E. Petersson, Analysis of crack formation and crack growth in concrete by means of fracture mechanics and finite elements, Cem. Concr. Res. 6 (1976) 773–782.
[11] M. Elices, J. Planas, Material models (Chap. 3) in: L. Elfgren (Ed.), Fracture Mechanics of Concrete Structures, Chapman & Hall, London, 1989, pp. 16–66.
[12] M. Elices, J. Planas, G.V. Guinea, Modeling cracking in rocks and cementitious materials, in: H.P. Rosmanith (Ed.), Fracture and Damage of Concrete and Rock, E&FN Spoon, London, 1993, pp. 3–33.
[13] RILEM TC 50 FCM Draft Recommendation, Determination of the fracture energy of mortar and concrete by means of three-point bend tests on notched beams, Mater. Struct. 18 (106) (1985) 285–290.
[14] G.V. Guinea, J. Planas, M. Elices, Measurement of the fracture energy using three-point bend tests: 1. Influence of experimental procedures, Mater. Struct. 25 (1992) 212–218.
[15] J. Planas, M. Elices, G.V. Guinea, Measurement of the fracture energy using three-point bend tests: 2. Influence of bulk energy dissipation, Mater. Struct. 25 (1992) 305–312.
[16] M. Elices, G.V. Guinea, J. Planas, Measurement of the fracture energy using three-point bend tests: 3. Influence of cutting the P–δ tail, Mater. Struct. 25 (1992) 327–334.
[17] G.V. Guinea, J. Planas, M. Elices, A general bilinear fit for the softening curve of concrete, Mater. Struct. 27 (1994) 99–105.
[18] C. Rocco, G.V. Guinea, J. Planas, M. Elices, Size effect and boundary conditions in the Brazilian test: Theoretical analysis, Mater. Struct. 32 (1999) 437–444.
[19] C. Rocco, G.V. Guinea, J. Planas, M. Elices, Size effect and boundary conditions in the Brazilian test: Experimental verification, Mater. Struct. 32 (1999) 210–217.
[20] T.R. Thomas, Rough Surfaces, Imperial College Press, London, 1999.
[21] K.M. El-Sayed, G.V. Guinea, C. Rocco, J. Planas, M. Elices, Influence of aggregate shape on the fracture behaviour of concrete, in: H. Mihashi, K. Rokugo (Eds.), Fracture Mechanics of Concrete Structures, Aedificatio Publishers, Freiburg, Germany, 1998, pp. 181–192.
[22] F.H. Wittmann, K. Rokugo, E. Bruhwiler, H. Mihashi, P. Simoni, Fracture energy and strain softening of concrete as determined by means of compact tension specimens, Mater. Struct. 21 (1988) 21–32.
[23] K. Rokugo, M. Iwasa, T. Suzuki, W. Koyanagi, Testing methods to determine tensile strain softening curve and fracture energy of concrete, in: H. Mihashi, H. Takahashi, F.H. Wittmann (Eds.), Fracture Toughness and Fracture Energy: Test Methods for Concrete and Rock, Balkema, Rotterdam, 1989, pp. 153–163.